PERGAMON

International Journal of Solids and Structures 39 (2002) 3057–3077

INTERNATIONAL JOURNAL OF SOLIDS and STRUCTURES

www.elsevier.com/locate/ijsolstr

High-order behavior of fully bonded and delaminated circular sandwich plates with laminated face sheets and a "soft" core

O. Rabinovitch [a], Y. Frostig [b,*]

[a] *Center for Composite Materials, University of Delaware, Newark, DE 19716, USA*
[b] *Faculty of Civil Engineering, Technion—Israel Institute of Technology, Haifa 32000, Israel*

Received 3 March 2001

Abstract

The bending behavior of circular, fully or partially bonded (delaminated), sandwich plates with a "soft" core and composite laminated face sheets of general layup is investigated. The analytical model derived follows the principles of the High-Order Sandwich Plate Theory and it is based on equilibrium and compatibility requirements. The variational principle of virtual work is employed for the derivation of the field equations along with the boundary and continuity conditions. The delamination considered forms a penny shaped disbonded zone, in which the delaminated faces can slip horizontally with respect one to another, yet they may be in contact accommodating vertical normal compressive stresses. The core is assumed a 3D elastic medium and the composite face sheets are modeled using the classical lamination theory, which yields coordinate dependent constitutive relations. The governing equations take the form of partial differential equations with variable coefficients. The solution procedure adopts the Galerkin method with truncated Fourier series in the circumferential direction and the multiple-points shooting method in the radial direction. Numerical results concerning typical fully and partially bonded sandwich plates are presented and discussed. The results reveal the effect of the anisotropy of the face sheets on the response of the structure and the influence of the delaminated area on the behavior of the sandwich plate. © 2002 Published by Elsevier Science Ltd.

Keywords: Sandwich plate; High order theory; Closed form solution; Compressible core; Delaminations; Composite laminates

1. Introduction

Advanced sandwich structures provide unique solutions in many fields of aerospace, mechanical, civil, and marine engineering. They combine materials to optimize the use of their different properties by bonding high strength and stiffness face sheets to a low-density and low-strength core. In many practical applications, the use of sandwich structures includes circular sandwich plates, while in other cases, the analysis of

* Corresponding author. Tel.: +972-4-8293-046; fax: +972-4-8323-433.
E-mail address: cvrfros@techunix.technion.ac.il (Y. Frostig).

0020-7683/02/$ - see front matter © 2002 Published by Elsevier Science Ltd.
PII: S0020-7683(02)00239-1

circular sandwich plates is required as a part of a sub-structuring (localization) process that enables detail investigation of localized effects in large-scale structures. Modern sandwich panels are made of a low-density flexible core and laminated composite face sheets. However, the laminated materials are usually made of *rectilinear orthotropic* plies whereas cylindrical orthotropic laminates that meet the circular geometry of the plate are not applicable. The use of such laminates in circular applications yields mechanical properties that depend on the circumferential coordinate and significantly complicates both the analysis and the design of such sandwich plates. In addition, the use of low strength core materials makes these structural members vulnerable to localized effects and manufacturing faults. One of these faults is involved with disbonding of the face sheets from the core. Such imperfection affects both the localized response of the plate through stress concentrations at the delamination's edge, and its overall bending behavior through lack of composite action of the various constituents.

The linear and nonlinear behavior of various types of sandwich panels with incompressible (rigid) cores has been widely investigated in the past years. Summaries of the general approaches are found in the classical textbooks of Plantema (1966), Allen (1969), and Zenkert (1995). Recent comprehensive reviews that present various analytical and computational models for sandwich structures are presented by Noor et al. (1996) and Librescu and Hause (2000). A broad range of theoretical and numerical models for the analysis of circular sandwich panels has been developed in the past years. A simplified and axisymmetric model in which the governing and equilibrium equations are derived based on the Reissner–Mindlin shear deformation plate theory was presented by Wang (1995a,b). A similar approach has been used by Demsetz and Gibson (1987) for weight minimization for a given flexural stiffness of the circular plate. The axisymmetric large amplitude free vibration of circular sandwich plates has been investigated by Du (1994) and Du and Li (2000). However, these models are limited to axisymmetric or isotropic behavior of the plate, to membrane action with no bending effects in the face sheets, and to incompressible cores. Higher order behavior and localized effects induced due to the circumferential anisotropy of laminated face sheets and due to flexibility of the core are not accounted for in these approaches. A different model has been presented by Bofilios and Lyrintzis (1992) for the investigation of the dynamic response of circular sandwich plates. This model accounts for the vertical compressibility of the core and for nonaxisymmetric effects, yet it ignores the shear deformations of the core and the membrane (inplane) action of the face sheets.

Recently, Frostig et al. (1992) and Frostig and Baruch (1992) have developed a general high-order theory for the analysis of sandwich panels and plates. The High-Order Sandwich Plate Theory (HSAPT) has been used extensively to model buckling and nonlinear response (Frostig, 1998; Sokolinski and Frostig, 1999), vibrations (Frostig and Baruch, 1994), and stress concentrations in general (Frostig, 1993; Frostig and Rabinovitch, 2000). In this theory, the high order and the localized effects are results of the closed form solution of the mathematical model and no presumptions are imposed on the distribution of the deformations through the thickness of the core. The theory accounts for the vertical flexibility of the core along with its shear flexibility, and it is valid for a broad range of sandwich structures.

Although the problem of localized debonding of the face-sheets from the core is extremely important, only a few analytical and experimental studies of such structures exist. These studies were discussed in Frostig (1992) and Frostig and Sokolinsky (1999), and most of them are devoted to the overall behavior of the delaminated panel and to its critical compression capacity (see for instance Zenkert, 1991; Somers et al., 1991; Lin et al., 1996). Investigation of more localized effects at the edge of the delaminated region using fracture mechanics criteria based on FE analysis was presented by Falk (1994). This study revealed the stress concentrations that arise in the close vicinity of the edge of the delaminated region and demonstrates their crucial influence on the safety of the structural members.

In this paper, the concepts of the HSAPT are adopted for the analysis of fully and partially bonded (delaminated) circular sandwich plates that consists of composite laminated faces with a general layup and

a compressible "soft" core. The model adopts the classical plate theory and uses the Bernoulli–Euler assumption for the behavior of the composite laminated face sheets. The constitutive relations for the face sheets are general, thus they can take any arbitrary layup (stacking sequence). The core is modeled as a 3D linear elastic continuum, possessing shear and vertical normal rigidities only, while its inplane radial and circumferential rigidities and its inplane shear rigidity are neglected (see Frostig et al., 1992; Frostig and Baruch, 1994). In addition, it is assumed that the deformations are small, the loads are applied only at the face sheets, and perfect bonding exists between the various constituents within the fully bonded region. Therefore, the core–face sheets interfaces are capable of resisting shear and vertical normal stresses. In the delaminated region, it is assumed that the disbonded faces are free of shear stresses (thus they may slip one with respect to another), but can accommodate vertical normal stresses if contact between them exists. Finally, it is assumed that the delamination exist prior to loading and does not expand as a result of the stresses involved.

The mathematical formulation uses the variational principle of virtual work for the derivation of the field equations along with the various boundary and continuity conditions. The formulation also includes the closed-form solution of the stress and deformation fields within the core and the generalized constitutive relations for the composite laminated face sheets. These constitutive relations are applicable to any general layup of rectilinear layers and yield equivalent rigidities that are functions of the circumferential coordinate. The governing equations of the fully or partially bonded regions form a set of partial differential equations with variable coefficients. The solution procedure uses the Galerkin method in the circumferential direction, and the multiple-points shooting method in the radial direction, whereas the distinction between delaminated regions with or without contact is conducted iteratively. Numerical investigation of the behavior of a typical circular sandwich plate with cross-ply laminated face sheets and a compressible core is presented. In addition, the influence of a localized circular delamination at the core–face sheet interface on the localized and overall behavior of the plate is investigated. A summary and conclusions appear in the sequel.

2. Mathematical formulation

The mathematical formulation includes the derivation of the field equations along with the boundary and continuity conditions, the constitutive relations, the stress and deformation fields of the core, and the governing equations. The geometry, notation, and sign convention of the coordinates, loads, stresses, and stress resultants appear in Fig. 1. Note that once a delamination has occurred, it divides the plate into two characteristic regions, namely: a fully bonded region and a delaminated one. Furthermore, within the delaminated region itself, a distinction is made between a delamination with interfacial vertical contact and a delamination without such contact (see Fig. 1(c)). The mathematical formulation presented ahead focuses on the fully bonded region, whereas the field and governing equations of the delaminated regions are derived by degenerating the equations of the fully bonded one.

2.1. Fully bonded region—field equations

The Field equations along with the boundary and continuity conditions are derived via the variational principle of potential energy minimization that requires

$$\delta(U + V) = 0 \tag{1}$$

where U and V are the internal potential energy and the potential energy of the external loads, respectively, and δ is the variational operator.

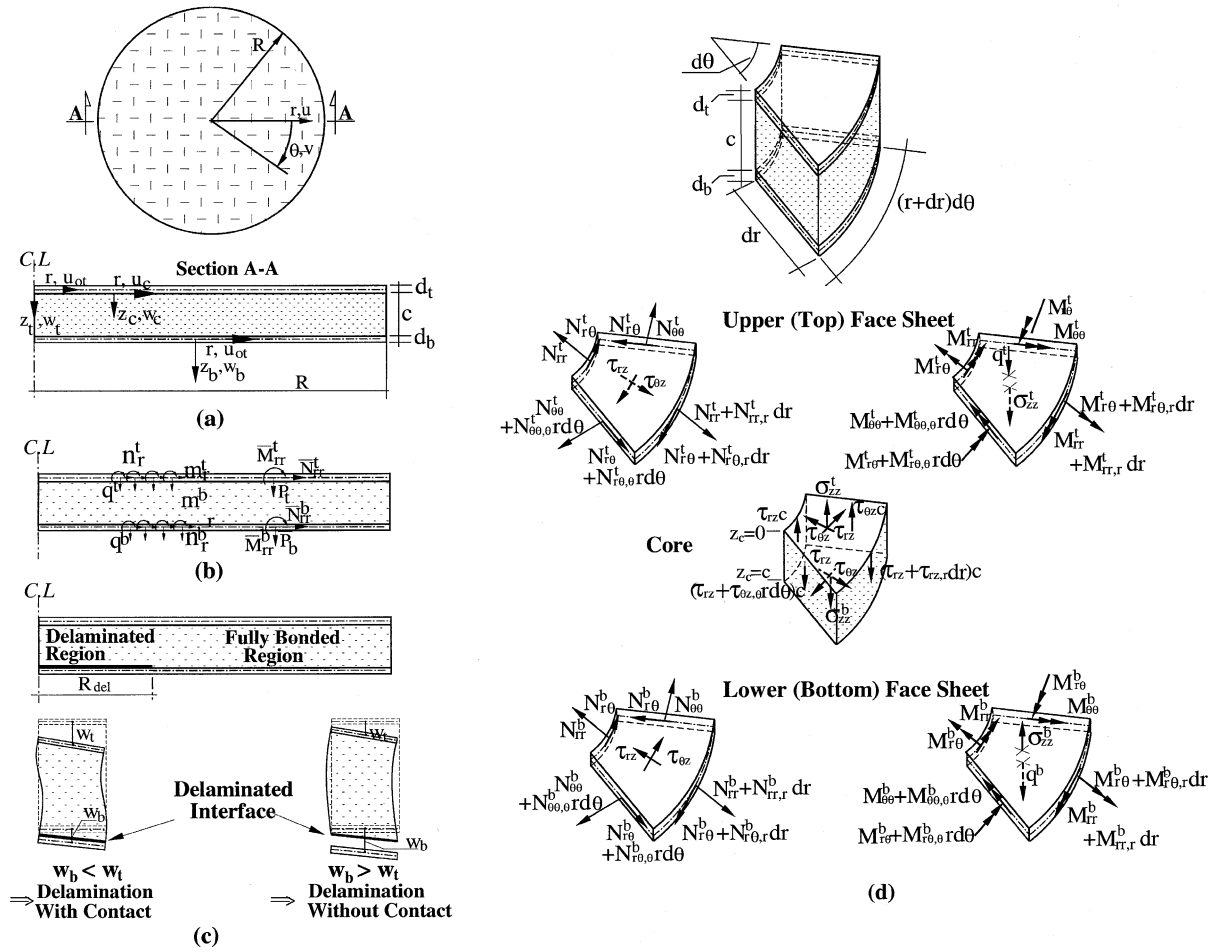

Fig. 1. Geometry, loads, sign convention, stress resultants and type of delaminations: (a) geometry, notations, and sign conventions; (b) loads; (c) types of delaminated regions; (d) stresses and stress resultants.

The first variation of the internal energy, in terms of the stresses and strains in the various constituents of the fully bonded region, read:

$$\delta U = \int_{v_t} \left(\sigma^t_{rr}\delta\varepsilon^t_{rr} + \sigma^t_{\theta\theta}\delta\varepsilon^t_{\theta\theta} + \tau^t_{r\theta}\delta\gamma^t_{r\theta}\right)\mathrm{d}v_t + \int_{v_b} \left(\sigma^b_{rr}\delta\varepsilon^b_{rr} + \sigma^b_{\theta\theta}\delta\varepsilon^b_{\theta\theta} + \tau^b_{r\theta}\delta\gamma^b_{r\theta}\right)\mathrm{d}v_b + \int_{v_c} (\tau_{rz}\delta\gamma_{rz} + \tau_{\theta z}\delta\gamma_{\theta z} + \sigma_{zz}\delta\varepsilon_{zz})\mathrm{d}v_c \tag{2}$$

where σ^i_{rr}, $\sigma^i_{\theta\theta}$ and ε^i_{rr}, $\varepsilon^i_{\theta\theta}$ are the stresses and strains in the radial and circumferential directions in the upper $(i = t)$ and the lower $(i = b)$ face sheets, respectively; $\tau^i_{r\theta}$, and $\gamma^i_{r\theta}$ are the inplane shear stress and strain in the face sheets, respectively; τ_{rz}, $\tau_{\theta z}$ and γ_{rz}, $\gamma_{\theta z}$ are the out-of-plane shear stresses and shear angles of the core, respectively; σ_{zz} and ε_{zz} are normal stress and strain in the vertical direction in the core; v_t, v_b and v_c are the volume of the upper and lower face sheets and the core, respectively; and $\mathrm{d}v$ denotes an infinitesimal volume segment, see Fig. 1.

The first variation of the potential energy of the external loads equals:

$$\begin{aligned}\delta V = &-\int_0^{2\pi}\left[\int_{r=0}^{r=R}\left(n_r^t\delta u_{0t}+n_\theta^t\delta v_{0t}+q^t\delta w_t+m_r^t\delta w_{t,r}+m_\theta^t\frac{\delta w_{t,\theta}}{r}\right)r\,\mathrm{d}r\right]\mathrm{d}\theta\\ &-\int_0^{2\pi}\left[\int_{r=0}^{r=R}\left(n_r^b\delta u_{0b}+n_\theta^b\delta v_{0b}+q^b\delta w_b+m_r^b\delta w_{b,r}+m_\theta^b\frac{\delta w_{b,\theta}}{r}\right)r\,\mathrm{d}r\right]\mathrm{d}\theta\\ &-\int_0^{2\pi}\left[\sum_{j=1}^{NC}\int_{r=0}^{r=R}\left(\overline{N}_{rrj}^t\delta u_{0t}+\overline{N}_{r\theta j}^t\delta v_{0t}+\overline{P}_j^t\delta w_t+\overline{M}_{rrj}^t\delta w_{t,r}+\overline{M}_{\theta\theta j}^t\frac{\delta w_{t,\theta}}{r}\right)\delta_{\mathrm{D}}(r-r_j)r\,\mathrm{d}r\right]\mathrm{d}\theta\\ &-\int_0^{2\pi}\left[\sum_{j=1}^{NC}\int_{r=0}^{r=R}\left(\overline{N}_{rrj}^b\delta u_{0b}+\overline{N}_{r\theta j}^b\delta v_{0b}+\overline{P}_j^b\delta w_b+\overline{M}_{rrj}^b\delta w_{b,r}+\overline{M}_{\theta\theta j}^b\frac{\delta w_{b,\theta}}{r}\right)\delta_{\mathrm{D}}(r-r_j)r\,\mathrm{d}r\right]\mathrm{d}\theta\end{aligned} \tag{3}$$

where n_r^i and n_θ^i are the external inplane loads in the radial and circumferential direction distributed over the area of the upper $(i=t)$ or the lower $(i=b)$ face sheets, respectively; m_r^i and m_θ^i $(i=t,b)$ are the external distributed bending moments in the radial and circumferential directions, respectively; q^i $(i=t,b)$ are distributed out-of-plane loads; $\overline{N}_{rrj}^i$, $\overline{N}_{r\theta j}^i$, $\overline{P}_j^i$, $\overline{M}_{rrj}^i$, $\overline{M}_{\theta\theta j}^i$ $(i=t,b)$ are the external loads and bending moments uniformly distributed along a circle of radius $r=r_j$; δ_{D} is the delta of Dirac function; NC is the number of circular line loads; u_{0i}, v_{0i}, and $w_{i,}$ $(i=t,b)$ are the radial, circumferential, and vertical displacements of the face sheets, respectively; and $(\,)_{,j}$ denotes partial derivative with respect to the coordinate j $(j=r,\theta)$.

The kinematic relations for the face sheets assuming small deformation and negligible shear effects read $(i=t,b)$

$$u_i(r,\theta,z_i)=u_{0i}(r,\theta)-z_iw_{i,r}(r,\theta),\quad v_i(r,\theta,z_i)=v_{0i}(r,\theta)-z_i\frac{w_{i,r}(r,\theta)}{r},\quad w_i(r,\theta,z_i)=w_i(r,\theta)\quad(i=t,b) \tag{4}$$

$$\varepsilon_{rr}^i(r,\theta,z_i)=\varepsilon_{0rr}^i(r,\theta)+z_i\chi_{rr}^i(r,\theta),\quad \varepsilon_{0rr}^i(r,\theta)=u_{0i,r},\quad \chi_{rr}^i(r,\theta)=-w_{i,rr}\quad(i=t,b) \tag{5}$$

$$\varepsilon_{\theta\theta}^i(r,\theta,z_i)=\varepsilon_{0\theta\theta}^i(r,\theta)+z_i\chi_{\theta\theta}^i(r,\theta),\quad \varepsilon_{0\theta\theta}^i(r,\theta)=\frac{v_{0i,\theta}}{r}+\frac{u_{0i}}{r},\quad \chi_{\theta\theta}^i(r,\theta)=-\left(\frac{w_{i,\theta\theta}}{r^2}+\frac{w_{i,r}}{r}\right)\quad(i=t,b) \tag{6}$$

$$\gamma_{r\theta}^i(r,\theta,z_i)=\gamma_{0r\theta}^i(r,\theta)+z_i\chi_{r\theta}^i(r,\theta),\quad \gamma_{0r\theta}^i(r,\theta)=\frac{u_{0i,\theta}}{r}-\frac{v_{0i}}{r}+v_{0i,r},\quad \chi_{r\theta}^i(r,\theta)=-2\left(\frac{w_{i,r\theta}}{r}+\frac{w_{i,\theta}}{r^2}\right)\quad(i=t,b) \tag{7}$$

where ε_{0kl}^i, γ_{0kl}^i, χ_{kl}^i $(k,l=r,\theta;\ i=t,b)$ are the inplane normal strains, the inplane shear angle, and the curvatures, respectively, of the upper and lower face sheets. Note that the vertical coordinate z_i $(i=t,b)$ is measured form the midplane of each face sheet downward, independently, and the circumferential coordinate, θ, is measured clockwise, see Fig. 1.

The kinematic relations for the core are based on 3D linear elasticity assuming small deformations and read

$$\begin{aligned}&\varepsilon_{zz}(r,\theta,z_c)=w_{c,z}(r,\theta,z_c),\quad \gamma_{rz}(r,\theta,z_c)=u_{c,z}(r,\theta,z_c)+w_{c,r}(r,\theta,z_c),\\ &\gamma_{\theta z}(r,\theta,z_c)=v_{c,z}(r,\theta,z_c)+\frac{w_{c,\theta}(r,\theta,z_c)}{r}\end{aligned} \tag{8}$$

where u_c, v_c, and w_c are the radial, circumferential, and vertical displacements of the core, respectively.

The compatibility conditions require perfect bonding at the upper and lower core–face sheet interfaces. Hence, they read

$$w_c(r,\theta,z_c=0)=w_t(r,\theta),\quad w_c(r,\theta,z_c=c)=w_b(r,\theta) \tag{9}$$

$$u_c(r,\theta,z_c=0)=u_{0t}(r,\theta)-\frac{d_t}{2}w_{t,r} \tag{10a}$$

$$u_c(r,\theta,z_c=c)=u_{0b}(r,\theta)+\frac{d_b}{2}w_{b,r} \tag{10b}$$

$$v_c(r,\theta,z_c=0)=v_{0t}(r,\theta)-\frac{d_t}{2}\frac{w_{t,\theta}}{r} \tag{11a}$$

$$v_c(r,\theta,z_c=c)=v_{0b}(r,\theta)+\frac{d_b}{2}\frac{w_{b,\theta}}{r} \tag{11b}$$

where c is the depth of the core; d_i $(i=t,b)$ are the depths of the upper and lower face sheets; and z_c is the vertical coordinate of the core measured from the upper core–face sheet interface downward, thus $z_c=0$ and $z_c=c$ refer to the upper and the lower core–face sheet interfaces respectively, see Fig. 1. Notice that the above compatibility conditions are imposed only in the fully bonded region. In the delaminated region, the disbonded constituents are free to slip horizontally with respect to one another, thus the compatibility conditions, Eqs. (10a), (10b), (11a) and (11b), at the delaminated interface are released. Yet, if the delaminated face sheet and the adjacent core remain in contact vertically ("delamination with contact"), the vertical compatibility condition of Eq. (9) must be fulfilled, while in the case of delamination without interfacial contact this condition is released as well.

Integration of the stresses through the depth of the face sheets defines the internal stress resultants as follows:

$$\begin{aligned} N^i_{kk}&=\int_{-d_i/2}^{d_i/2}\sigma^i_{kk}\,\mathrm{d}z_i,\quad M^i_{kk}=\int_{-d_i/2}^{d_i/2}\sigma^i_{kk}z_i\,\mathrm{d}z_i,\quad (i=t,b)\ (k=r,\theta)\\ N^i_{r\theta}&=\int_{-d_i/2}^{d_i/2}\tau^i_{r\theta}\,\mathrm{d}z_i,\quad M^i_{r\theta}=\int_{-d_i/2}^{d_i/2}-\tau^i_{r\theta}z_i\,\mathrm{d}z_i,\quad (i=t,b)\end{aligned} \tag{12}$$

where N^i_{rr}, $N^i_{\theta\theta}$ $(i=t,b)$ are the inplane radial and circumferential stress resultants; $N^i_{r\theta}$ $(i=t,b)$ are the inplane shear stress resultants; M^i_{rr}, $M^i_{\theta\theta}$ $(i=t,b)$ are the radial and circumferential bending moments; and $M^i_{r\theta}$ $(i=t,b)$ are the twisting moments.

The field equations are derived using the variational principle, Eqs. (1)–(3), along with the kinematic relations, Eqs. (4)–(7), the compatibility conditions, Eqs. (9), (10a), (10b), (11a) and (11b), and the internal stress resultants, Eq. (12). After some algebraic manipulation the field equations of the fully bonded region read

$$\left(N^t_{rr}\cdot r\right)_{,r}-N^t_{\theta\theta}+N^t_{r\theta,\theta}+(\tau_{rz}\cdot r)+n^t_r\cdot r=0 \tag{13}$$

$$\left(N^b_{rr}\cdot r\right)_{,r}-N^b_{\theta\theta}+N^b_{r\theta,\theta}-(\tau_{rz}\cdot r)+n^b_r\cdot r=0 \tag{14}$$

$$\left(N^t_{r\theta}\cdot r\right)_{,r}+N^t_{\theta\theta,\theta}+N^t_{r\theta}+(\tau_{\theta z}\cdot r)+n^t_\theta\cdot r=0 \tag{15}$$

$$\left(N^b_{r\theta}\cdot r\right)_{,r}+N^b_{\theta\theta,\theta}+N^b_{r\theta}-(\tau_{\theta z}\cdot r)+n^b_\theta\cdot r=0 \tag{16}$$

$$\left(M^t_{rr}\cdot r\right)_{,rr}-M^t_{\theta\theta,r}+\frac{M^t_{\theta\theta,\theta\theta}}{r}+2M^t_{r\theta,r\theta}+2\frac{M^t_{r\theta,\theta}}{r}+\sigma_{zz}(z_c=0)r+\frac{d_t}{2}(\tau_{rz}\cdot r)_{,r}+\frac{d_t}{2}\tau_{\theta z,\theta}+q^t\cdot r-\left(m^t_r\cdot r\right)_{,r}-m^t_{\theta,\theta}=0 \tag{17}$$

$$\left(M^b_{rr}\cdot r\right)_{,rr}-M^b_{\theta\theta,r}+\frac{M^b_{\theta\theta,\theta\theta}}{r}+2M^b_{r\theta,r\theta}+2\frac{M^b_{r\theta,\theta}}{r}-\sigma_{zz}(z_c=0)r+\frac{d_b}{2}(\tau_{rz}\cdot r)_{,r}+\frac{d_b}{2}\cdot\tau_{\theta z,\theta}+q^b\cdot r-\left(m^b_r\cdot r\right)_{,r}-m^b_{\theta,\theta}=0 \tag{18}$$

$$\sigma_{zz,z}\cdot r+(\tau_{rz}\cdot r)_{,r}+\tau_{\theta z,\theta}=0 \tag{19}$$

$$\tau_{rz,z}=0 \tag{20}$$

$$\tau_{\theta z,z}=0 \tag{21}$$

2.2. Fully bonded region—core stress and displacement fields

The stress and displacement fields of the core are derived using the equilibrium equations, the compatibility requirements, the kinematic relations, and linear and elastic constitutive relation. The solution of Eqs. (20) and (21) reveal uniform shear stress distributions through the thickness of the core, thus

$$\tau_{rz}(r,\theta,z_c)=\tau_{rz}(r,\theta) \tag{22}$$

$$\tau_{\theta z}(r,\theta,z_c)=\tau_{\theta z}(r,\theta) \tag{23}$$

The solution of the vertical equilibrium equation, (19), along with the shear stress distributions of Eqs. (23) and (24), yields the vertical normal stress field that reads

$$\sigma_{zz}(r,\theta,z_c)=\frac{w_b-w_t}{c}E_c-\left(\frac{(\tau_{rz}\cdot r)_{,r}}{r}+\frac{\tau_{\theta z,\theta}}{r}\right)\left(z_c-\frac{c}{2}\right) \tag{24}$$

where E_c is the elastic modulus of the core in the vertical direction. The vertical displacement field of the core is defined using the vertical normal stress distribution, Eq. (24), along with the compatibility of the vertical displacement requirement, Eq. (9). Hence, it takes the following form:

$$w_c(r,\theta,z_c)=\left(\frac{(\tau_{rz}\cdot r)_{,r}}{2rE_c}+\frac{\tau_{\theta z}}{2rE_c}\right)\left(cz_c-z_c^2\right)+\frac{(w_b-w_t)}{c}z_c+w_t \tag{25}$$

The radial and the circumferential displacement fields are determined using Eq. (25), the constitutive and kinematic relations, and the perfect bond compatibility conditions at the interfaces, Eqs. (10a) and (11a). Thus, after integration through the depth of the core, the radial and the circumferential displacement fields equal

$$\begin{aligned}u_c(r,\theta,z_c)=u_{0t}-\frac{d_t}{2}w_{t,r}+\left(\tau_{rz,rr}+\frac{\tau_{rz,r}}{r}-\frac{\tau_{rz}}{r^2}+\frac{\tau_{\theta z,\theta r}}{r}-\frac{\tau_{\theta z,\theta}}{r^2}\right)\frac{z_c^3}{6E_c}\\+\left[\frac{w_{t,r}-w_{b,r}}{2c}+\frac{c}{4E_c}\left(\frac{\tau_{rz}}{r^2}-\frac{\tau_{rz,r}}{r}-\tau_{rz,rr}+\frac{\tau_{\theta z,\theta}}{r^2}-\frac{\tau_{\theta z,\theta r}}{r}\right)\right]z_c^2+\left(\frac{\tau_{rz}}{G_c}-w_{t,r}\right)z_c\end{aligned} \tag{26}$$

$$\begin{aligned}v_c(r,\theta,z_c)=v_{0t}-\frac{d_t}{2}\frac{w_{t,\theta}}{r}+\left(\frac{\tau_{\theta z,\theta\theta}}{r^2}+\frac{\tau_{rz,r\theta}}{r}+\frac{\tau_{rz,\theta}}{r^2}\right)\frac{z_c^3}{6E_c}+\left[\frac{w_{t,\theta}-w_{b,\theta}}{2rc}-\frac{c}{4E_c}\left(\frac{\tau_{rz,\theta}}{r^2}+\frac{\tau_{\theta z,\theta\theta}}{r^2}-\frac{\tau_{rz,\theta r}}{r}\right)\right]z_c^2\\+\left(\frac{\tau_{\theta z}}{G_c}-\frac{w_{t,\theta}}{r}\right)z_c\end{aligned} \tag{27}$$

where G_c is the shear modulus of the core. Note that the stress and deformation fields of Eqs. (22)–(26), (28) have nonlinear patterns through the depth of the core and actually describe the high order effects in the core.

2.3. Delaminated region—field equations

In the case of a *delamination with contact*, the shear stresses at the disbonded interface vanish; yet, it can accommodate vertical normal stresses. Accordingly, the solution of Eqs. (20) and (21), along with the requirement of zero sheer stresses at the delaminated interface, reveal that the shear stresses are nil throughout the entire depth of the core

$$\tau_{rz}(r,\theta,z_c) = 0 \tag{28}$$

$$\tau_{\theta z}(r,\theta,z_c) = 0 \tag{29}$$

Introducing the resulting nullified shear stress fields into Eq. (19) yields a uniform vertical normal stress distribution through the depth of the core as follows:

$$\sigma^0_{zz} = \sigma_{zz}(r,\theta) = \frac{w_b - w_t}{c} E_c \tag{30}$$

where σ^0_{zz} denotes the constant vertical normal stress field through the thickness of the core. Consequently, the field equations of the upper and lower face sheets in the delaminated region when interfacial contact exists are

$$\left(N^t_{rr}\cdot r\right)_{,r} - N^t_{\theta\theta} + N^t_{r\theta,\theta} + n^t_r \cdot r = 0 \tag{31}$$

$$\left(N^b_{rr}\cdot r\right)_{,r} - N^b_{\theta\theta} + N^b_{r\theta,\theta} + n^b_r \cdot r = 0 \tag{32}$$

$$\left(N^t_{r\theta}\cdot r\right)_{,r} + N^t_{\theta\theta,\theta} + N^t_{r\theta} + n^t_\theta \cdot r = 0 \tag{33}$$

$$\left(N^b_{r\theta}\cdot r\right)_{,r} + N^b_{\theta\theta,\theta} + N^b_{r\theta} + n^b_\theta \cdot r = 0 \tag{34}$$

$$\left(M^t_{rr}\cdot r\right)_{,rr} - M^t_{\theta\theta,r} + \frac{M^t_{\theta\theta,\theta\theta}}{r} + 2M^t_{r\theta,r\theta} + 2\frac{M^t_{r\theta,\theta}}{r} + \sigma^0_{zz} r + q^t r - \left(m^t_r \cdot r\right)_{,r} - m^t_{\theta,\theta} = 0 \tag{35}$$

$$\left(M^b_{rr}\cdot r\right)_{,rr} - M^b_{\theta\theta,r} + \frac{M^b_{\theta\theta,\theta\theta}}{r} + 2M^b_{r\theta,r\theta} + 2\frac{M^b_{r\theta,\theta}}{r} - \sigma^0_{zz} r + q^b r - \left(m^b_r \cdot r\right)_{,r} - m^b_{\theta,\theta} = 0 \tag{36}$$

In the case of a delamination *without contact*, both shear and the vertical normal stresses at the disbonded interface vanish. Eqs. (19)–(21) and the stress-free face conditions at the delaminated interface yield null shear and vertical stress distributions through the height of the core, $\tau_{rz} = \tau_{\theta z} = \sigma^0_{zz} = 0$. Hence, the resulting field equations of the upper and lower face sheets include Eqs. (31)–(34), and Eqs. (35)–(36) after omitting the terms multiplied by σ^0_{zz}.

2.4. Boundary and continuity conditions

The variational principle yields nine boundary conditions at the edges of the fully bonded region and eighteen continuity conditions within this region. The boundary conditions are:

$$\lambda \cdot N^i_{rr} - \overline{N}^i_{rr} = 0 \quad \text{or} \quad u_{0i} = \bar{u}_{0i} \tag{37}$$

$$\lambda \cdot N^i_{r\theta} - \overline{N}^i_{r\theta} = 0 \quad \text{or} \quad v_{0i} = \bar{v}_{0i} \tag{38}$$

$$\lambda\left[\frac{M^i_{rr} + 2M^i_{r\theta,\theta} - M^i_{\theta\theta}}{r} + M^i_{rr,r} + \frac{d_i}{2}\tau_{rz}\right] - \overline{P}^i - m^i_r = 0 \quad \text{or} \quad w_i = \bar{w}_i \tag{39}$$

$$-\lambda \cdot M^i_{rr} - \overline{M}^i_{rr} = 0 \quad \text{or} \quad w_{i,r} = \bar{w}_{i,r} \tag{40}$$

where $\overline{N}^i_{rr}$, $\overline{N}^i_{r\theta}$, $\overline{P}^i$ and $\overline{M}^i_{rr}$ $(i = t, b)$ are external loads and bending moments exerted along the edge of the upper and lower face sheets, $\bar{u}_{0i}$, $\bar{v}_{0i}$, $\bar{w}_i$ and $\bar{w}_{i,r}$ are prescribed deformations and rotations, $\lambda = 1$ at the outer edges, and $\lambda = -1$ at the center.

The boundary conditions at any point through the thickness of the core read:

$$\tau_{rz}(\theta) = 0 \quad \text{or} \quad w_c(\theta, z_c) = \bar{w}_c(\theta, z_c) \tag{41}$$

where $\bar{w}_c(\theta, z_c)$ is a prescribed vertical displacement through the thickness of the core.

The continuity conditions require continuity of the displacements and slopes along with equilibrium of the internal forces and the external loads. The continuity conditions of the upper and lower face sheets at $r = r_j$ within the bonded region are:

$$u^{(-)}_{0i} = u^{(+)}_{0i}, \quad v^{(-)}_{0i} = v^{(+)}_{0i}, \quad w^{(-)}_i = w^{(+)}_i, \quad w^{(-)}_{i,r} = w^{(+)}_{i,r} \tag{42}$$

$$N^{i(-)}_{rr} - N^{i(+)}_{rr} = \overline{N}^i_{rrj} \tag{43}$$

$$N^{i(-)}_{r\theta} - N^{i(+)}_{r\theta} = \overline{N}^i_{r\theta j} \tag{44}$$

$$\left[\frac{M^{i(-)}_{rr} + 2M^{i(-)}_{r\theta,\theta} - M^{i(-)}_{\theta\theta}}{r_j} + M^{i(-)}_{rr,r} + Y_i \cdot \tau^{i(-)}_{rz}\right] - \left[\frac{M^{i(+)}_{rr} + 2M^{i(+)}_{r\theta,\theta} - M^{i(+)}_{\theta\theta}}{r_j} + M^{i(+)}_{rr,r} + Y_i \cdot \tau^{i(+)}_{rz}\right] = \overline{P}^i_j \tag{45}$$

$$-M^{i(-)}_{rr} + M^{i(+)}_{rr} = \overline{M}^i_{rrj} \tag{46}$$

And the continuity conditions of the core are:

$$w^{(-)}_c(r_j, \theta, z_c) = w^{(+)}_c(r_j, \theta, z_c) \tag{47}$$

$$\tau^{(-)}_{rz}(\theta) = \tau^{(+)}_{rz}(\theta) \tag{48}$$

In the delaminated region (with and without contact), the variational principle yields eight boundary and sixteen continuity conditions. The boundary conditions at the edges of these regions consist of Eqs. (37)–(40) without the terms that include τ_{rz}. The continuity conditions within the delaminated region include Eqs. (42)–(46) without the terms that include τ_{rz}.

3. Constitutive relations

The generalized constitutive relations for the upper and lower composite laminated face sheets read

$$\begin{bmatrix} \mathbf{N}^i \\ \mathbf{M}^i \end{bmatrix} = \begin{bmatrix} \mathbf{A}^i & \mathbf{B}^i \\ \mathbf{B}^i & \mathbf{D}^i \end{bmatrix} \begin{bmatrix} \boldsymbol{\varepsilon}^i \\ \boldsymbol{\chi}^i \end{bmatrix} \quad (i = t, b) \tag{49}$$

where $\mathbf{N}^i$, $\mathbf{M}^i$, $\boldsymbol{\varepsilon}^i$, $\boldsymbol{\chi}^i$ are the vectors of the internal stress resultants and the midplane surface strain and curvature, respectively, and $\mathbf{A}^i$, $\mathbf{B}^i$, and $\mathbf{D}^i$ are the extensional, extension-flexural, and flexural rigidities of the upper ($i = t$) and the lower ($i = b$) face sheets, respectively (see Jones, 1975)).

In the general case of the circular laminated plate, these rigidities are θ-dependent and equal:

$$C_{11}(\theta) = C_{11}(0)m^4 + 2(C_{12}(0) + 2C_{66}(0))n^2m^2 + C_{22}(0)n^4 \tag{50}$$

$$C_{12}(\theta) = (C_{11}(0) + C_{22}(0) - 4C_{66}(0))n^2m^2 + C_{12}(0)\left(n^4 + m^4\right) \tag{51}$$

$$C_{22}(\theta) = C_{11}(0)n^4 + 2(C_{12}(0) + 2C_{66}(0))n^2m^2 + C_{22}(0)m^4 \tag{52}$$

$$C_{16}(\theta) = (C_{11}(0) - C_{12}(0) - 2C_{66}(0))nm^3 + (C_{12}(0) - C_{22}(0) + 2C_{66}(0))mn^3 \tag{53}$$

$$C_{26}(\theta) = (C_{11}(0) - C_{12}(0) - 2C_{66}(0))mn^3 + (C_{12}(0) - C_{22}(0) + 2C_{66}(0))nm^3 \tag{54}$$

$$C_{66}(\theta) = (C_{11}(0) + C_{22}(0) - 2C_{12}(0) - 2C_{66}(0))m^2m^2 + C_{66}(0)(n^4 + m^4) \tag{55}$$

where $m = \cos(\theta)$ and $n = \sin(\theta)$; $C_{jk}(\theta) = A^i_{jk}(\theta)$, $B^i_{jk}(\theta)$, $D^i_{jk}(\theta)$ $(i = t, b)$ are the θ-dependent rigidities; $C_{jk}(0)$ refers to the rigidities evaluated at $\theta = 0$ and the subscripts $j, k = 1, 2, 6$ refer to the radial, the circumferential, and the inplane shear/twisting directions, respectively. Note that in this case, Eqs. (50)–(55) represent the θ-dependent rigidities of the circular plate, and not the classical stiffness transformations.

4. Governing equations and solutions

The governing equations of the fully bonded and the delaminated regions are derived using the field equations along with the constitutive relations and the stress fields of the core. The seventh and eighth equations of the fully bonded region are determined by imposing the compatibility requirement of the radial and circumferential displacements at the lower core–face sheet interface, Eqs. (10b) and (11b). This is achieved using the displacement fields of the core, Eqs. (26) and (28), evaluated at $z_c = c$. Thus, the compatibility equations of the fully bonded region read:

$$\left(\frac{\tau_{rz}}{r^2} - \frac{\tau_{rz,r}}{r} - \tau_{rz,rr} + \frac{\tau_{\theta z,\theta}}{r^2} - \frac{\tau_{\theta z,\theta r}}{r}\right)\frac{c^3}{12E_c} - \left(\frac{c + d_t}{2}\right)w_{t,r} - \left(\frac{c + d_b}{2}\right)w_{b,r} + \frac{\tau_{rz}}{G_c}c + u_{0t} - u_{0b} = 0 \tag{56}$$

$$\left(-\frac{\tau_{rz,\theta}}{r^2} - \frac{\tau_{\theta z,\theta\theta}}{r^2} - \frac{\tau_{rz,\theta r}}{r}\right)\frac{c^3}{12E_c} - \left(\frac{c + d_t}{2}\right)\frac{w_{t,\theta}}{r} - \left(\frac{c + d_b}{2}\right)\frac{w_{b,\theta}}{r} + \frac{\tau_{\theta z}}{G_c}c + v_{0t} - v_{0b} = 0 \tag{57}$$

In the delaminated regions, the disbonded faces are free to slip one with respect to another, hence no compatibility requirements are imposed on the horizontal displacements.

Finally, the formulation yields a set of six partial differential governing equations in the delaminated region and eight equations in the fully bonded region. These equations are stated in terms of the unknown displacements and the unknown shear stresses of the core. However, the equations are rather lengthy and cumbersome, thus, they are not presented here explicitly. For brevity, the governing equations are referred here through a differential operator. In the fully bonded region the differential operator reads:

$$\mathbf{L}\psi_m(\boldsymbol{\psi}(r, \theta)) - f_m = 0 \quad m = 1, \ldots, 8 \tag{58}$$

where

$$\boldsymbol{\psi} = \{u_{0t}(r, \theta), u_{0b}(r, \theta), v_{0t}(r, \theta), v_{0b}(r, \theta), w_t(r, \theta), w_b(r, \theta), \tau_{rz}(r, \theta), \tau_{\theta z}(r, \theta)\}^{\mathrm{T}}$$

is the vector of unknowns; f_m denotes the external distributed loads and moments; $\mathbf{L}\psi_m$ with $m = 1,\ldots,6$ is the differential operator of the equilibrium equations (Eqs. (13)–(18) in terms of the unknowns), and $\mathbf{L}\psi_m$ with $m = 7,\ldots,8$ refers to the compatibility equations of the fully bonded region (Eqs. (56) and (57)). In the delaminated region, the last two terms in the vector of the unknowns are omitted and the operator refers only to the six equilibrium equations.

The boundary/continuity conditions are also presented in the form of a differential operator that in the fully bonded region equals:

$$\mathbf{L}_{\mathbf{BC}_k}(\boldsymbol{\psi}(\theta)) - F_k = 0 \quad k = 1,\ldots,9 \tag{59}$$

where $\mathbf{L}_{\mathbf{BC}_k}$ $(k = 1,\ldots,9)$ refers to Eqs. (37)–(41), and F_k denotes the external loads and moments of the natural boundary conditions or the prescribed deformation fields of the essential boundary conditions. The differential operator of the continuity conditions at $r = r_j$ within the fully bonded region reads:

$$\mathbf{L}_{\mathbf{CC}_l}\big(\boldsymbol{\psi}(r_j,\theta)\big) - P_l = 0 \quad l = 1,\ldots,18 \tag{60}$$

where $\mathbf{L}_{\mathbf{CC}_l}$ $(l = 1,\ldots,18)$ is the differential operator and P_l denotes the circular line loads and moments for the natural continuity conditions (Eqs. (43)–(47)), and $P_l = 0$ is used in the essential boundary conditions (Eqs. (42) and (48)). Again here, the eight boundary and conditions and the sixteen continuity conditions of the delaminated region are derived by omitting the last two terms in $\boldsymbol{\psi}$ and using Eqs. (59) and (60) with $(k = 1,\ldots,8)$ and $(l = 1,\ldots,16)$, respectively.

It was noted earlier that the size of the delaminated region is assumed not to grow under loading, yet the type of delamination (with or without contact) is determined iteratively. The type of delamination is assumed a priori, and validated through the results. If the presumption turns to be incorrect, reanalysis with the other type of delamination is conducted. In most practical cases, this iterative procedure converges very fast and it is not involved with major computational efforts.

The resulting governing equations form three different sets of partial differential equations with coefficients that are functions of both the radial and the circumferential coordinates. Hence, a closed-form type of solution does not exist and an approximated solution approach based on the Galerkin method in the circumferential direction and the multiple-points shooting method in the radial direction is employed. The approximated solution takes the form of truncated Fourier series and in the case of axisymmetric out-of-plane loading it equals

$$u_{0t}(r,\theta) \approx \sum_{n=0}^{N} u_{0t}^n(r)\cos(n\theta), \quad u_{0b}(r,\theta) \approx \sum_{n=0}^{N} u_{0b}^n(r)\cos(n\theta) \tag{61}$$

$$v_{0t}(r,\theta) \approx \sum_{n=0}^{N} v_{0t}^n(r)\sin(n\theta), \quad v_{0b}(r,\theta) \approx \sum_{n=0}^{N} v_{0b}^n(r)\sin(n\theta) \tag{62}$$

$$w_t(r,\theta) \approx \sum_{n=0}^{N} w_t^n(r)\cos(n\theta), \quad w_b(r,\theta) \approx \sum_{n=0}^{N} w_b^n(r)\cos(n\theta) \tag{63}$$

$$\tau_{rz}(r,\theta) \approx \sum_{n=0}^{N} \tau_{rz}^n(r)\cos(n\theta), \quad \tau_{\theta z}(r,\theta) \approx \sum_{n=0}^{N} \tau_{\theta z}^n(r)\sin(n\theta) \tag{64}$$

where $u_{0t}^n(r)$, $u_{0b}^n(r)$, $v_{0t}^n(r)$, $v_{0b}^n(r)$, $w_t^n(r)$, $w_b^n(r)$, $\tau_{rz}^n(r)$, and $\tau_{\theta z}^n(r)$ are unknown functions of the radial coordinate only, and N denotes the number of terms in the series. The partial differential equations are thus replaced by a set of ordinary differential equations resulting from the Galerkin integrals that read:

$$\int_0^{2\pi} ((\mathbf{L}\boldsymbol{\psi}_m(\boldsymbol{\psi}(r,\theta)) - f_m)g_n(\theta))\,\mathrm{d}\theta = 0 \quad m = 1,\ldots,8 \text{ or } 6;\ n = 0,\ldots,N \tag{65}$$

where $g_n(\theta)$ is determined in accordance with the variational term that multiplies the various equilibrium and compatibility equations, i.e., $g_n(\theta) = \cos(n\theta)$ for $m = 1, 2, 5, 6, 7$ and $g_n(\theta) = \sin(n\theta)$ for $m = 3, 4, 8$.

Accordingly, the Galerkin procedure is applied to the boundary and continuity conditions of Eqs. (59) and (60) as follows:

$$\int_0^{2\pi} ((\mathbf{L}_{\mathbf{BC}_k}(\boldsymbol{\psi}(\theta)) - F_k)g_n(\theta))\,\mathrm{d}\theta = 0 \quad k = 1,\ldots,9 \quad \text{or} \quad 8;\ n = 0,\ldots,N \tag{66}$$

$$\int_0^{2\pi} ((\mathbf{L}_{\mathbf{CC}_l}(\boldsymbol{\psi}(\theta)) - P_l)g_n(\theta))\,\mathrm{d}\theta = 0 \quad l = 1,\ldots,18 \quad \text{or} \quad 16;\ n = 0,\ldots,N \tag{67}$$

where in the case of natural boundary/continuity conditions $g_n(\theta)$ is defined by the variational term that multiplies each condition. In the case of essential conditions, $g_n(\theta)$ is set equal to the θ-dependent function that appears in the approximated solution, Eqs. (61)–(64).

The Galerkin procedure employed in the circumferential direction yields a set of ordinary differential equations with r-dependent coefficients. These equations are further transformed into a set of coupled first order equations that along with the boundary/continuity conditions are solved numerically using the multiple-points shooting method (see Stoer and Bulirsch, 1993). The accuracy of the numerical method is examined through the convergence of the solution with an increased number of terms in the truncated Fourier series and with refinement of the multi-points shooting mesh. The fulfillment of the overall vertical equilibrium is also examined and a condition of relative error smaller than 10^{-6} has been adopted.

5. Numerical study

The behavior of a circular sandwich plate, loaded by a localized distributed load at its center and simply supported only at the lower face sheet, is investigated for three particular cases. In the first case, the sandwich plate is fully bonded and the localized load is exerted at the upper face sheet. In the second and the third cases, a penny shaped delamination located at the lower core–face interface at the center of the plate is considered. In the second case studied, the load is exerted at the upper face sheet, thus a type of delamination "with contact" is expected. In the third case the lower face sheet is loaded, thus a type of delamination "without contact" is likely to occur. The geometrical layout and the loading scheme of the investigated bonded and delaminated plates appear in Fig. 2. The mechanical properties of the core and the composite laminated face sheets appear in Table 1. Note that the loads, the boundary conditions, and the mechanical properties of the core are symmetrical about the z-axis (axisymmetric). In addition, the layup used for the laminated composite face sheets is symmetrical about the mid-height plane of each face sheet, thus the **B** matrix vanishes. However, the rigidities of the upper and lower face sheets are θ-dependent. In the following sections, the influence of the anisotropy of the laminated face sheets of the behavior of the sandwich structure is investigated.

Five terms truncated Fourier series ($n = 0,\ldots,4$) are used for the depiction of the structural response in the circumferential direction. Yet, due to the 0°/180° symmetry of the laminated face sheets, only even values of n yield nonvanishing equations. Thus, the order of the resulting problem is fifty. In the delaminated region (with or without contact), the order of the resulting problem is reduced to 44. The results are presented in terms of the displacements and internal stress resultant in the face sheets, the shear stresses in the core, and the vertical normal stresses in the upper and lower core–face interfaces.

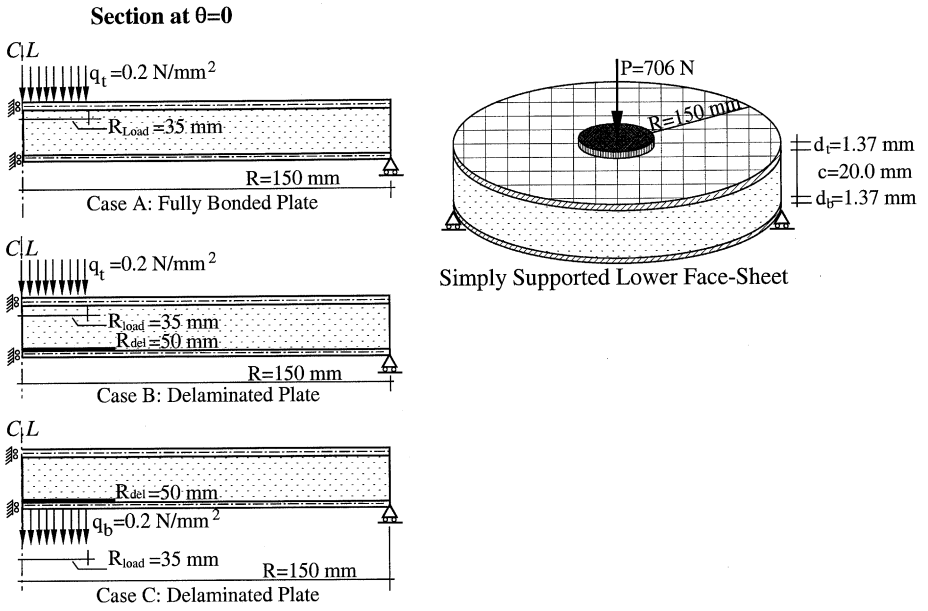

Fig. 2. Numerical example: geometry and loading schemes.

Table 1
Material properties

Isotropic materials	E (GPa)		G (GPa)	v (–)	c (mm)	
Core	52.5		21.0	0.25	20	
Composite materials	E_{11} (GPa)[a]	E_{22} (GPa)[a]	G_{12} (GPa)[a]	v_{12} (–)[a]	t_{ply} (mm)	Stacking sequence
Face sheets	165	9.7	4.8	0.31	0.152	$[0,90,0]_{3S}$

[a] Here the 1, 2 notation refers to directions parallel and perpendicular to the fiber's directions of each orthotropic ply, respectively.

5.1. Case A: Fully bonded sandwich plate

The first example investigates a fully bonded sandwich panel subjected to a localized load exerted at its upper face (see Fig. 2, case A). The results in terms of the radial, circumferential, and vertical deflections appear in Fig. 3 and reveal that even though the loads and the boundary conditions are axisymmetric, the resulting displacement fields depend on both the radial and the circumferential coordinates. Notice that the vertical deflections exhibit a somewhat reduced dependence on the circumferential coordinate, as compared to the radial or the circumferential ones. This effect implies that the strong anisotropy of the face sheets is damped by the compliant core. Also, notice that the vertical deflections of the upper and the lower face sheets are alike throughout most of the plate's area. This excludes the area in the close vicinity of the localized load and near the edge of the plate, where only the lower face sheet is supported while the upper one is free. These trends are attributed to the compressibility of the "soft" core and to the high order effects that are accounted for in the proposed approach.

The inplane and moment stress resultants in the upper and lower face sheets of the fully bonded sandwich plate appear in Fig. 4. The results reveal that both the inplane and the moment radial stress

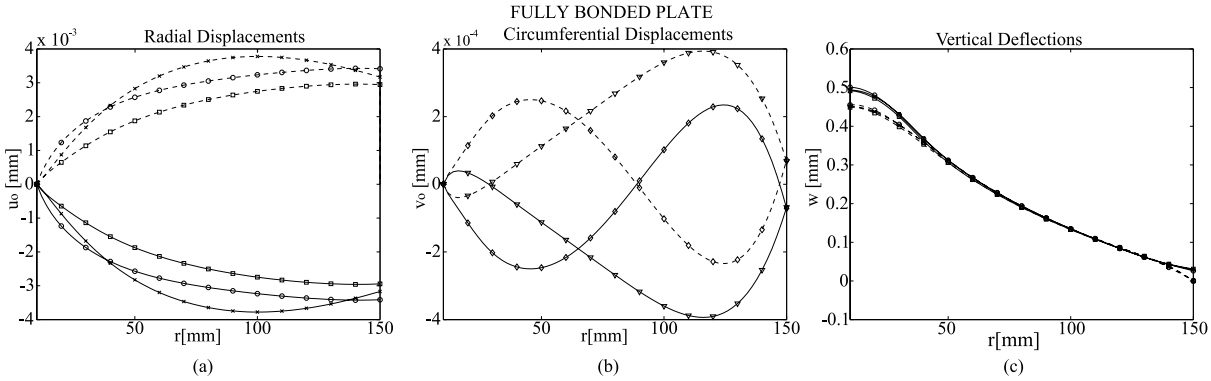

Fig. 3. Displacements of a fully bonded sandwich plate: (a) radial displacements; (b) circumferential displacements; (c) vertical displacements. (Legend: (—) upper face sheet, (- - -) lower face sheet, (○) $\theta = 0°$, (◇) $\theta = 22.5°$, (×) $\theta = 45°$, (▽) $\theta = 67.5°$, (□) $\theta = 90°$).

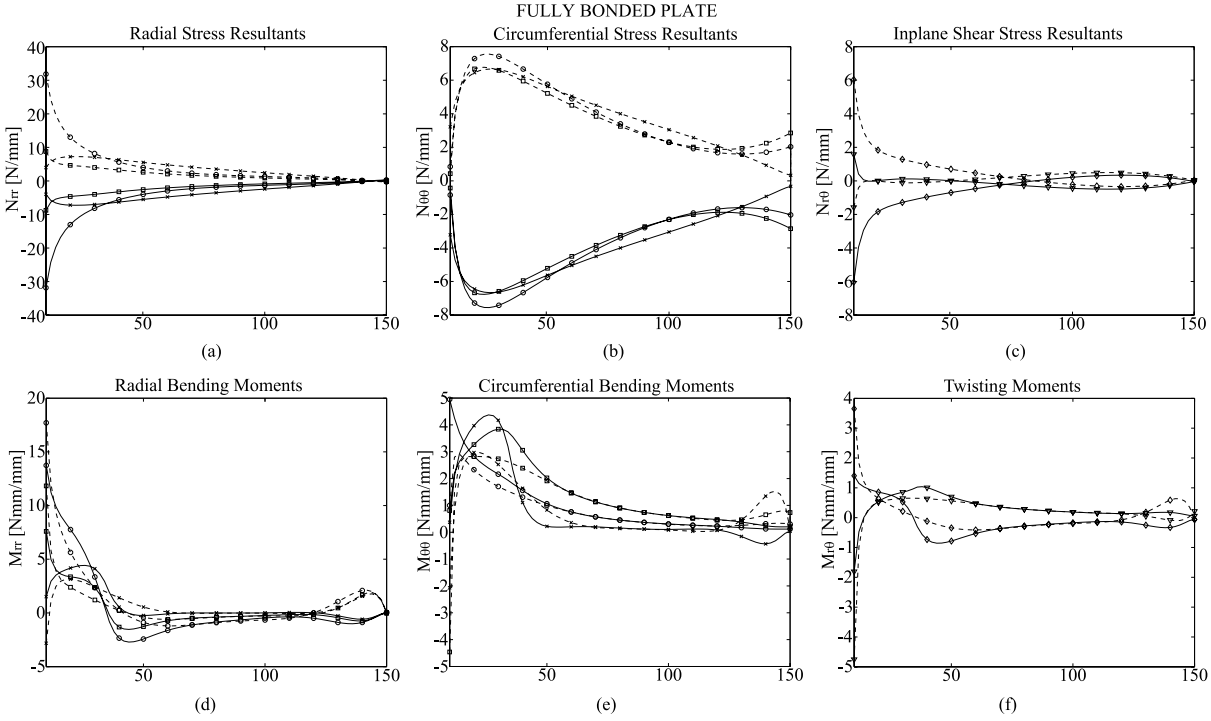

Fig. 4. Internal stress resultants in upper and lower face sheets of a fully bonded sandwich plate: (a–c) inplane stress resultants; (d–f) moment stress resultants. (Legend: (—) upper face sheet, (- - -) lower face sheet, (○) $\theta = 0°$, (◇) $\theta = 22.5°$, (×) $\theta = 45°$, (▽) $\theta = 67.5°$, (□) $\theta = 90°$).

resultants, which form the main load transfer mechanism of the sandwich plate, are considerably larger than the circumferential and the shear/twisting stress resultants. The results also indicate that the internal stress resultants are affected by the anisotropy of the laminated face sheets. The radial stress resultants at $\theta = 0°$, which is the stiffest direction of the face sheet, are significantly larger than those observed at

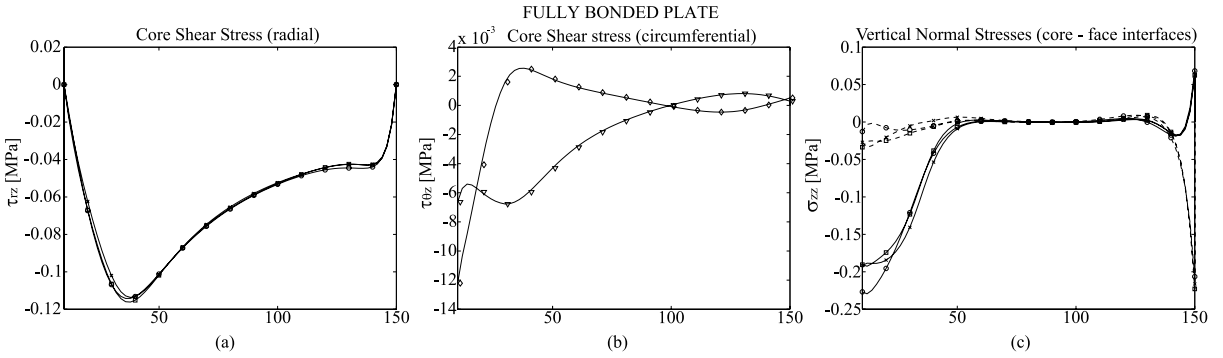

Fig. 5. Shear stresses in the core and vertical normal stresses in the core–face sheet interfaces of a fully bonded sandwich plate: (a) shear stresses on radial face, τ_{rz}; (b) shear stresses on circumferential face, τ_{θ_z}; (c) vertical normal stresses. (Legend: (—) upper face sheet, (- - -) lower face sheet, (○) $\theta = 0°$, (◇) $\theta = 22.5°$, (×) $\theta = 45°$, (▽) $\theta = 67.5°$, (□) $\theta = 90°$).

$\theta = 90°$, which is the most compliant direction. Hence, the composite action of the sandwich, which is defined as the ratio of the global bending moment carried in the form of an inplane tensile and compressive couple in the face sheets, is enhanced in the stiffer direction and reduced in the more compliant ones. The results presented in Fig. 4 also reveal that the boundary conditions at the edge of the plate $N^i_{rr}(\theta, R) = N^i_{r\theta}(\theta, R) = M^i_{rr}(\theta, R) = 0$ $(i = t, b)$ are almost perfectly fulfilled, although imposed only in an integral "weak" form via the Galerkin method, Eq. (66).

The shear stresses on the radial (τ_{rz}) and on the circumferential (τ_{θ_z}) faces of the core and the vertical normal stresses at the upper and lower core–face sheet interfaces appear in Fig. 5(a)–(c), respectively. Fig. 5(a) and (b) indicate that the shear stresses on the radial face of the core are considerably larger than those on the circumferential one, and their dependence on the circumferential coordinate is weaker. The distributions of the interfacial normal stresses reveal the localized stress concentrations that arise in the vicinity of the localized load and near the edge of the plate. These localized effects are characterized by dissimilar stresses at the upper and the lower core–face interfaces resulting from the high shear gradients in these regions, see Eq. (26). It is important to emphasis that these localized effects that are predicted by the high-order theory (HSAPT) are among the major causes of damage or even premature failure of many types of sandwich structures. One of these damage patterns is associated with disbonding or delamination at the core–face interfaces. In the next sections, the influence of such a delamination on the overall and localized response of the sandwich structure is investigated.

5.2. Case B: Delaminated sandwich plate—upper face sheet loaded

In this case, the behavior of a delaminated sandwich plate with a "soft" core and laminated face sheets is investigated. The geometrical and mechanical properties of the plate and the loading scheme are identical with those of the plate in case A and appear in Fig. 2 and Table 1. However, in this case, a circular 50-mm-radius delamination is located in the center of the plate at the lower core–face interface (see Fig. 2, case B). In addition, the localized load is exerted at the upper face sheet; hence, a type of delamination "with contact" is initially presumed.

The results in terms of the displacement fields of the delaminated plate appear in Fig. 6 and reveal that the radial and circumferential displacements exhibit similar magnitudes and trends to those observed in the fully bonded plate. However, the vertical displacements are increased, and they are about twice the deflections in the fully bonded plate. This phenomenon is attributed to the lack of composite action of the upper and lower face sheets as a result of the null shear stresses in the delaminated region. The vertical

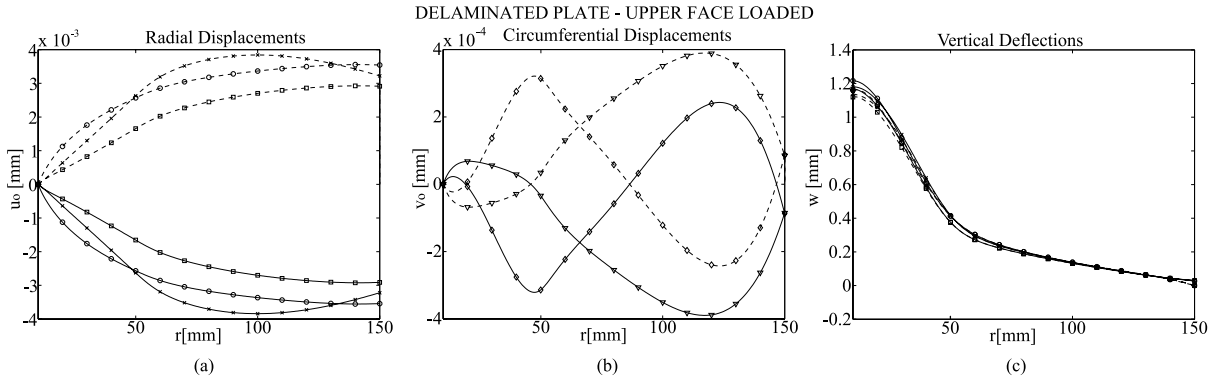

Fig. 6. Displacements of a delaminated sandwich plate loaded at its upper face: (a) radial displacements; (b) circumferential displacements; (c) vertical displacements. (Legend: (—) upper face sheet, (- - -) lower face sheet, (○) $\theta = 0°$, (◇) $\theta = 22.5°$, (×) $\theta = 45°$, (▽) $\theta = 67.5°$, (□) $\theta = 90°$).

displacement fields (Fig. 6(c)) also show that the deflections of the upper face sheet are larger than those of the lower one throughout the entire delaminated region. Hence, the assumption of delamination with vertical contact is justified and reanalysis is not required.

Additional results in terms of the internal inplane and moment stress resultants in the upper and lower face sheets of the delaminated sandwich plate are presented in Fig. 7. These results indicate that the radial and the shear stress resultants are reduced by about 15%, as compared with those of the fully bonded plate, whereas the circumferential resultants are not significantly changed (see Figs. 7(a)–(c) and 4(a)–(c)). Correspondingly, the moment stress resultants, and especially the radial bending moments near the center of the plate and near the edge of the delaminated region, are amplified by an order of magnitude, as compared with those observed in the fully bonded plate (see Figs. 7(d)–(f) and 4(d)–(f)). Hence, it can be concluded that the existence of a delaminated region at the center of the plate impairs the composite action of the sandwich structure. However, it appears that the delaminated plate is still capable of resisting the applied load and can still be considered as a functioning structural member.

The stress fields within the core of the delaminated plate appear in Fig. 8 and clearly show the null shear stresses and the constant through the thickness vertical normal stresses within the delaminated region. The results also reveal the high stress concentrations that arise in the vicinity of the delamination's edge. This stress concentration is governed by the rapid growth of the shear stresses that yields vertical normal compressive stresses at the upper core–face sheet interface and vertical normal tensile (peeling) stresses at the lower interface (see Fig. 8(c)). Notice that the stress concentrations near the edge of the delaminated region are significantly higher than those that arise near the edge of the plate. Furthermore, in many cases, the high peeling stresses that develop at the tip of delaminated zone are the main cause to the growth of the delaminated area, which might lead to failure of the entire sandwich plate.

5.3. Case C: Delaminated sandwich plate—lower face sheet loaded

The last case investigates the same delaminated sandwich plate studied in the previous section; yet, here the lower face sheet is loaded instead of the upper one (see Fig. 2, case C). Such configuration and loading scheme entail the presumption of a delamination "without contact". The radial, circumferential, and vertical displacements of this delaminated plate that appear in Fig. 9 clearly demonstrate the effect of this loading scheme on the behavior of the delaminated structure. Here, the radial and the circumferential displacements (Fig. 9(a) and (b)) are similar to those observed in cases A and B, but the vertical dis-

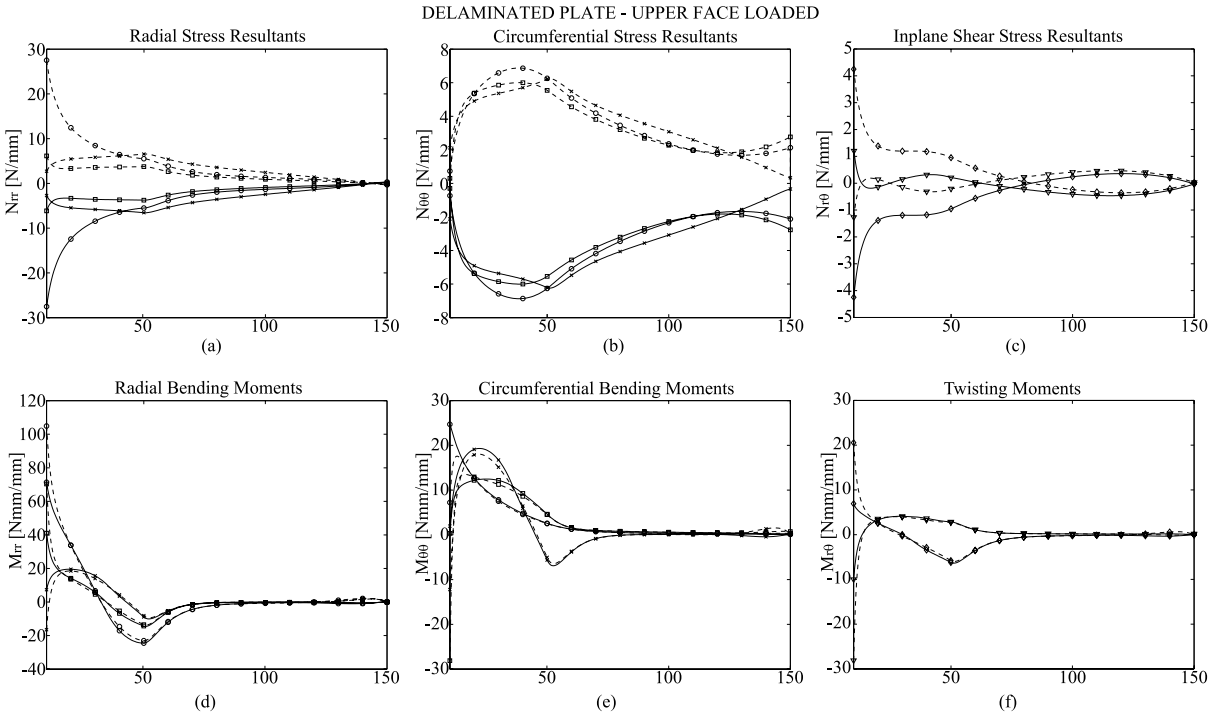

Fig. 7. Internal stress resultants in upper and lower face sheets of a delaminated sandwich plate loaded at its upper face: (a–c) inplane stress resultants; (d–f) moment stress resultants. (Legend: (—) upper face sheet, (- - -) lower face sheet, (○) $\theta = 0°$, (◇) $\theta = 22.5°$, (×) $\theta = 45°$, (▽) $\theta = 67.5°$, (□) $\theta = 90°$).

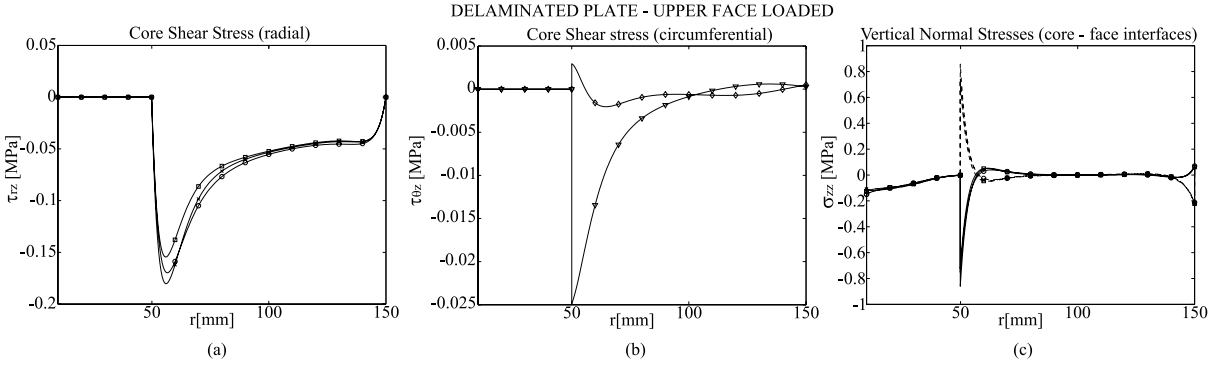

Fig. 8. Shear stresses in the core and vertical normal stresses in the core–face sheet interfaces of a delaminated sandwich plate loaded at its upper face: (a) shear stresses on radial face, τ_{rz}; (b) shear stresses on circumferential face, $\tau_{\theta z}$; (c) vertical normal stresses. (Legend: (—) upper face sheet, (- - -) lower face sheet, (○) $\theta = 0°$, (◇) $\theta = 22.5°$, (×) $\theta = 45°$, (▽) $\theta = 67.5°$, (□) $\theta = 90°$).

placements are significantly larger and equal about four times the vertical displacements observed in the fully bonded plate. The results also justify the initial assumption of a delamination without contact since the vertical displacements of the loaded lower face sheet are considerably larger than those of the upper one throughout the entire delaminated region.

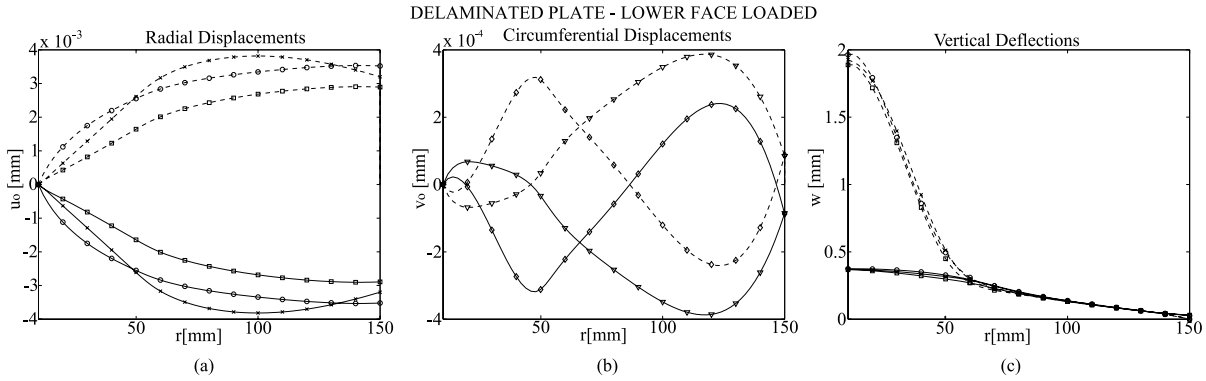

Fig. 9. Displacements of a delaminated sandwich plate loaded at its lower face: (a) radial displacements; (b) circumferential displacements; (c) vertical displacements. (Legend: (—) upper face sheet, (- - -) lower face sheet, (○) $\theta = 0°$, (◇) $\theta = 22.5°$, (×) $\theta = 45°$, (▽) $\theta = 67.5°$, (□) $\theta = 90°$).

Further results in terms of the inplane and moment stress resultants in the upper and lower face sheets appear in Fig. 10. The inplane radial, circumferential, and shear stress resultants are similar, both in trends and in magnitudes, to those observed in the fully bonded plate and are almost identical to those observed in the delaminated plate where interfacial contact exists. On the contrary, the radial and circumferential

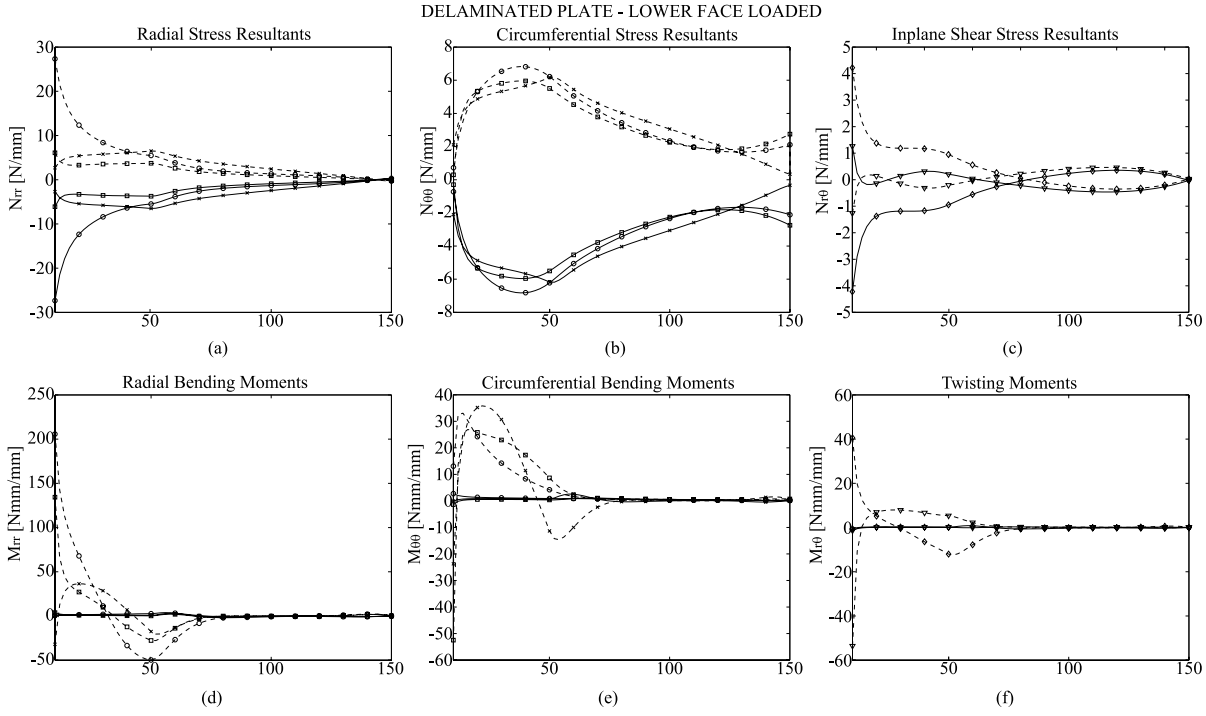

Fig. 10. Internal stress resultants in upper and lower face sheets of a delaminated sandwich plate loaded at its lower face: (a–c) inplane stress resultants; (d–f) moment stress resultants. (Legend: (—) upper face sheet, (- - -) lower face sheet, (○) $\theta = 0°$, (◇) $\theta = 22.5°$, (×) $\theta = 45°$, (▽) $\theta = 67.5°$, (□) $\theta = 90°$).

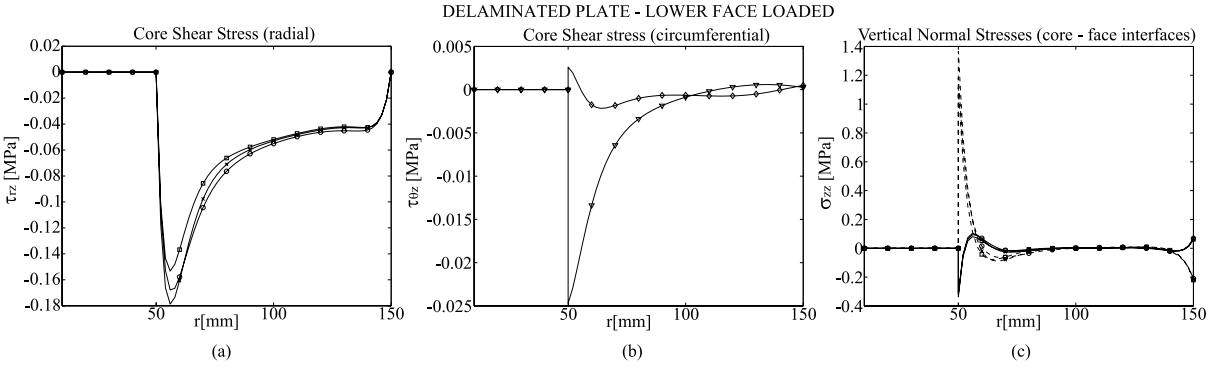

Fig. 11. Shear stresses in the core and vertical normal stresses in the core–face sheet interfaces of a delaminated sandwich plate loaded at its lower face: (a) shear stresses on radial face, τ_{rz}; (b) shear stresses on circumferential face, $\tau_{\theta z}$; (c) vertical normal stresses. (Legend: (—) upper face sheet, (- - -) lower face sheet, (○) $\theta = 0°$, (◇) $\theta = 22.5°$, (×) $\theta = 45°$, (▽) $\theta = 67.5°$, (□) $\theta = 90°$).

bending moments and the twisting moments in the loaded lower face sheet are considerably amplified, as compared with those observed in previous cases, whereas the moments in the upper face sheet are nearly nil throughout the delaminated region. This phenomenon implies that the load is carried only by the lower face sheet, while its collaboration with the upper face sheet is achieved only through the continuity requirements at the edge of the delaminated region.

The shear and vertical normal stress distributions that appear in Fig. 11 reveal that the stress concentrations that arise near the edge of the delaminated region, and especially the high peeling stresses, are also increased, as compared to the response of the fully bonded plate and the delaminated plate with contact. These stress distributions also reveal the null shear stresses and the null vertical normal stresses of the core within the delaminated region. Hence, the behavior of the delaminated region, in the case of delamination without contact, is that of two separate thin laminated plates interconnected only at the edge of the delaminated region. This configuration yields high stresses in the face sheets and high stress concentrations at the edge of the delaminated region that in many cases entail a total failure of the sandwich plate immediately with the formation of disbonded region.

6. Summary and conclusions

A systematic high-order approach for the analysis of circular, fully bonded or delaminated, sandwich plates with a soft core and laminated composite face sheets of general layup has been presented. The derived model follows the concept of the HSAPT that is based on equilibrium and compatibility requirements in every part of the structure. It allows the analysis of fully bonded as well as delaminated sandwich plates, with or without contact at the disbonded interfaces. The displacements and the stress fields of the compressible core are determined through the solution of its 3D elasticity field equations along with the kinematic and constitutive relations and are not postulated a priori. In addition, the model accounts for arbitrary layup for the laminated composite face sheets that may have any coordinate dependent mechanical properties.

The field equations and the corresponding boundary and continuity conditions have been derived via the variational principle of virtual work. The field equations, along with the coordinate dependent constitutive relations, the closed-form stress and displacement fields of the core, and the compatibility requirements yield a set of partial differential equations with variable coefficients. A solution procedure that adopts the

Galerkin method with truncated Fourier series in the circumferential direction and the multiple-points shooting method in the radial direction has been employed.

The capabilities of the proposed model have been demonstrated through the numerical investigation of three particular cases. In the first one, the influence of the anisotropy of the cross-ply laminated face sheets of the structural response of a fully bonded circular sandwich plate has been investigated. In the second case, the effect of a localized penny shaped delamination located at the lower core–face sheet interface on the behavior of a sandwich plate loaded at its upper face sheet has been investigated. The results in this case have revealed that this geometry and loading scheme yields a type of delamination "with contact", which is associated with constant through the depth of the core vertical compressive stress in the delaminated region. In the last case, the lower face sheet of the delaminated plate has been loaded, leading to a type of delamination "without contact."

The results have revealed that despite the fact that the layout, the loading, and the boundary conditions of the investigated sandwich plates are symmetrical about the z-axis (axisymmetric), the response of the structure is affected by the strong anisotropy of the laminated face sheets. However, it appears that these effects are somewhat damped by the compressible "soft" core. The comparison of the response of the delaminated plates with that of the fully bonded one has revealed that the disbonding at the core–face sheet interface impairs the composite action of the face sheets, reduces the efficiency of the sandwich structure, and is associated with high stress concentrations at the edge of the delaminated region. However, in the case of delamination with contact, the damaged structure is still capable of resisting the imposed load, while in the case of delamination without contact, the load is carried only by the loaded face sheet and failure of the structure is likely to occur. Furthermore, all these cases reveal that whenever sandwich structures are used, the localized effects in the form of high internal stress resultants in the face sheets and stress concentrations in the core are inevitable. Accurate prediction of these localized effects, which are one of the major causes of premature failure in such structures, is one of the major advantages of the proposed model.

Finally, it can be concluded that the presented high-order model can be effectively used to describe the behavior of circular bonded and delaminated sandwich plates of various layout and loading and it sets the basis for their effective design and safe use.

References

Allen, H.G., 1969. Analysis and Design of Structural Sandwich Panels. Pergamon Press, Oxford.

Bofilios, D.A., Lyrintzis, C.S., 1992. Response of double-wall (sandwich) circular plates to random excitations—analytical approach. Journal of Aircraft 29 (5), 932–938.

Demsetz, L.A., Gibson, L.J., 1987. Minimum weight design for stiffness in sandwich plates with rigid foam cores. Materials Science and Engineering 85 (1–2), 33–42.

Du, G., 1994. Large amplitude vibration of circular sandwich plates. Applied Mathematics and Mechanics (English Edition) 15 (5), 461–469.

Du, G., Li, H., 2000. Nonlinear vibration of circular sandwich plate under uniformed load. Applied Mathematics and Mechanics 21 (2), 217–226.

Falk, L., 1994. Foam core sandwich panels with interface disbonds. Composite Structures 28 (4), 481–490.

Frostig, Y., 1992. Behavior of delaminated sandwich beams with transversely flexible core—high order theory. Composite Structures 20 (1), 1–16.

Frostig, Y., 1993. On stress concentration in the bending of sandwich beams with transversely flexible core. Composite Structures 24, 161–169.

Frostig, Y., 1998. Buckling of sandwich panels with a transversely flexible core-high-order theory. International Journal of Solids and Structures 35 (3–4), 183–204.

Frostig, Y., Baruch, M., Vilnai, O., Sheinman, I., 1992. High-order theory for sandwich-beam bending with transversely flexible core. ASCE Journal of Engineering Mechanics 118 (5), 1026–1043.

Frostig, Y., Baruch, M., 1992. Localized load effects in high order bending of sandwich panels with flexible Core. ASCE Journal of Engineering Mechanics 122 (11), 1069–1076.

Frostig, Y., Baruch, M., 1994. Free vibration of sandwich beams with a transversely flexible core a high order approach. Journal of Sound and Vibration 176 (2), 195–208.

Frostig, Y., Rabinovitch, O., 2000. Behavior of sandwich panels with multi-skin construction or a multi-layered core—a high-order approach. Journal of Sandwich Structures and Materials 2 (3), 181–213.

Frostig, Y., Sokolinsky, V., 1999. Buckling of debonded (delaminated) sandwich panels with a transversely flexible core. ASME Proceeding, in Recent Advances in Mechanics of Aerospace Structures and Materials, G. Newaz (Ed.), ASME International Congress and Exposition, Nashville, Tennessee, USA, 14–19 November, pp. 23–40.

Jones, R.M., 1975. Mechanics of Composite Materials. Scripta Book Co., Washington, DC.

Librescu, L., Hause, T., 2000. Recent developments in the modeling and behavior of advanced sandwich constructions: a survey. Composite Structures 48 (1), 1–17.

Lin, C.C., Cheng, S.H., Wang, J.T.S., 1996. Local buckling of delaminated composite sandwich plates. AIAA Journal 30 (10), 2183–3176.

Noor, A.K., Burton, W.S., Bert, C.W., 1996. Computational models for sandwich panels and shells. Applied Mechanics Reviews 49, 155–199.

Plantema, F.J., 1966. Sandwich Construction. John Wiley & Sons, New York.

Sokolinski, V., Frostig, Y., 1999. Non-linear behavior of sandwich panels with a transversely flexible core—high-order theory approach. AIAA Journal 37 (11), 1474–1482.

Somers, M., Weller, T., Abramovich, H., 1991. Influence of predetermined delaminations on buckling and postbuckling behavior of composite sandwich beams. Composite Structures 17 (4), 295–329.

Stoer, J., Bulirsch, R., 1993. Introduction to Numerical Analysis. Springer-Verlag, New York, NY.

Wang, C.M., 1995a. Deflection of sandwich plates in terms of corresponding Kirchhoff plate solutions. Archive of Applied Mechanics 65 (6), 408–414.

Wang, C.M., 1995b. Buckling of polygonal and circular sandwich plates. AIAA Journal 33 (5), 962–964.

Zenkert, D., 1991. Strength of sandwich beams with interfacial debondings. Composite Structures 17 (4), 331–350.

Zenkert, D., 1995. An Introduction to Sandwich Construction. Chameleon Press Ltd., London.